Surface & Coatings Technology 219 (2013) 69–74

Contents lists available at SciVerse ScienceDirect

Surface & Coatings Technology

journal homepage: www.elsevier.com/locate/surfcoat

High-alloy martensite in the surfacing layer of hot-rolling supporting rollers during the tempering process

Jian Yang [a], Yulin Yang [b], Yefei Zhou [a], Xiaowen Qi [b], Xuejun Ren [c], Qingxiang Yang [a,*]

[a] State Key Laboratory of Metastable Materials Science and Technology, College of Materials Science and Engineering, Yanshan University, Qinhuangdao 066004, China
[b] College of Mechanical Engineering, Yanshan University, Qinhuangdao, 066004, China
[c] School of Engineering, Liverpool John Moores University, Liverpool L3 3AF, UK

ARTICLE INFO

Article history:
Received 30 October 2012
Accepted in revised form 4 January 2013
Available online 11 January 2013

Keywords:
High-alloy martensite
Tempering
Hot-rolling supporting roller
Weld surfacing

ABSTRACT

Flux-cored wire for surfacing hot-rolling supporting roller was developed and the specimens of surfacing layers were tempered at different temperatures. In order to characterize the high-alloy martensite in the surfacing layer during the tempering process, the microstructure and phase structure of the surfacing layer were analyzed, respectively. The nanoindentation hardness and phase transformation temperature of the high-alloy martensite were measured. The crystal structure of each phase was analyzed. The results show that the microstructure of the as-welded surfacing layer consists of martensite and retained austenite. Meanwhile, the high-alloy martensite with white reticular morphology is distributed on the crystal boundary. With increase of the tempering temperature, the high-alloy martensite disappears gradually, and the black reticular microstructure finally appears when the tempering temperature is 650 °C. The high-alloy martensite, whose average nanoindentation is 14.33 GPa, shows bulk morphology in field emission scanning electron microscope and starts to dissolve in the matrix at 420 °C. The contents of the alloy elements in the high-alloy martensite are higher than those in the normal one. However, the former decrease rapidly after tempering at 650 °C. The high-alloy martensite shows the body-centered tetragonal crystal structure, and the c-axis of the high-alloy martensite is longer than that of the normal one.

1. Introduction

Hot-rolling supporting roller is a key workpiece during rolling production, which plays an important role in supporting the hot-rolling work roller. Therefore, the quality of the hot-rolling supporting roller affects not only its service life, but also the quality and production efficiency of hot-rolled products indirectly [1].

During its work process, the hot-rolling supporting roller bears mechanical load, thermal load, and friction load. After being in service for a period of time, it may fail due to thermal fatigue [2] and excessive attrition [3].

The failed hot-rolling supporting roller can be repaired by the surfacing (surface-welding) method to restore its dimension and shape [4], and to obtain higher performance [5]. When traditional welding materials were employed for surfacing the failed hot-rolling supporting roller, higher strength and hardness of the as-welded surfacing layer can be obtained. However, after being tempered for some time, the hardness of the surfacing layer decreases largely [6], which can no longer meet the mechanical property requirements of the hot-rolling supporting roller [7].

R.R. DeAvillez [8] demonstrated that if large amount of alloy elements such as Cr, Mn, Mo, Ni, and V exist in the steel, the retained austenite and martensite exist stability in the surfacing layer during the tempering process, and dissolved until the higher temperature. S. Saduman [9] indicated that stabilized retained austenite and martensite ensured the steel with high anti-tempering properties, which keep its higher hardness when the hot-rolling supporting roller worked at higher temperature. Moreover, the mechanical properties such as strength [10], hardness [11] and corrosion resistance [12] of the martensite with high alloy content (high-alloy martensite) are higher than those of the normal martensite had been reported.

The development of the hot-rolling supporting roller material is characterized by the composition with higher alloy element content [13], specially with higher Cr content [14]. Therefore, based on the composition of the hot-rolling supporting roller, a new kind of flux-cored wire with high alloy element additive was developed. Then, the

Table 1
Chemical composition of steel H08A (wt.%).

C	Mn	Si	Cr	Ni	S	P	Fe
≤0.1	0.3–.5	≤0.03	≤0.2	≤0.3	≤0.03	≤0.03	Balance

* Corresponding author. Tel.: +86 3358387471.
E-mail address: qxyang@ysu.edu.cn (Q. Yang).

0257-8972/$ – see front matter © 2013 Elsevier B.V. All rights reserved.
http://dx.doi.org/10.1016/j.surfcoat.2013.01.006

Table 2
Chemical composition of steel Q235 (wt.%).

C	Si	Mn	P	S	Fe
≤0.18	0.12~0.30	0.35~0.80	≤0.04	≤0.04	Balance

Table 3
Chemical composition of the hardfacing metal (wt.%).

C	Si	P	S	Cr	Ni	Mo	V	Mn	Fe
0.186	0.94	0.0089	0.029	5.92	3.05	2.14	0.425	1.52	balance

surfacing layers were tempered at different temperatures. By observing the microstructure and analyzing the phase structure, the high-alloy martensite in the surfacing layer was characterized during the tempering process, which can provide theoretical foundation for developing a new kind of flux-cored wire for surfacing hot-rolling supporting roller.

2. Experimental procedure

2.1. Materials

Flux-cored wire for surfacing the hot-rolling supporting roller was manufactured. The core powders were composed of ferrosilicon, ferrochrome, ferromanganese, and so on. The outer steel of the wire was made of low carbon steel H08A manufactured by Tangshan Iron and Steel Company, with chemical composition listed in Table 1. During the production process of the flux-cored wire, the amount of coated flour is 46–48 wt.%, the dimension of the used core powder is 40–60 mesh, the width of steel band is 12 mm and the final diameter of the welding wire is 3.2 mm.

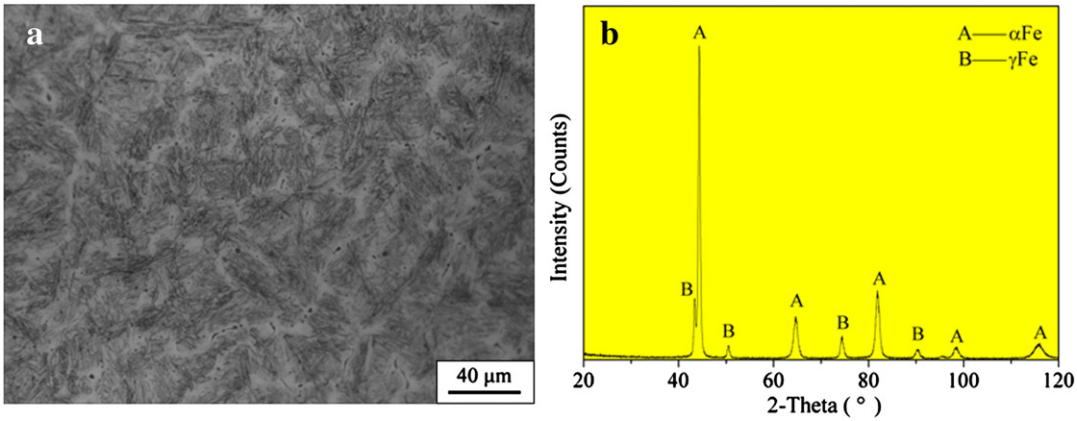

Fig. 1. a) Microstructure and b) XRD of the hardfacing metal as-welded.

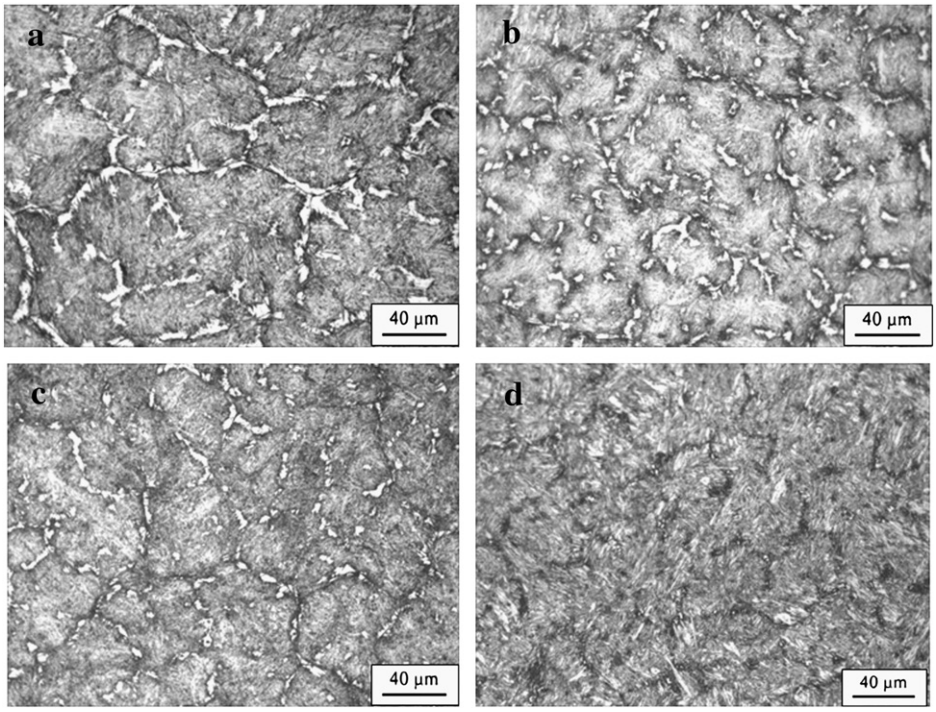

Fig. 2. Microstructures of the hardfacing metals tempered at a) 350 °C, b) 450 °C, c) 550 °C and d) 650 °C.

2.2. Experimental methods

Base metal for the welding surface was prepared from low carbon steel plate of Q235, whose chemical composition is listed in Table 2. Three layers were welded onto the surface of each specimen. The chemical composition of the surfacing layer is listed in Table 3.

In order to analyze the effect of the tempering temperature on the white reticular microstructure, the surfacing specimens were heated to 350 °C, 450 °C, 550 °C, and 650 °C respectively, and then cooled to ambient temperature in the furnace after holding for 120 min. After being metallographically polished, the surfacing layers were etched with 4% nitric acid alcohol. The microstructure of the specimen was characterized by an Axiovert 200 MAT optical microscope (OM) and a Hitachi S4800 field emission scanning electron microscope (FESEM) equipped with an energy dispersive X-ray spectrometry (EDS). The phase structure was determined by X-ray diffraction (XRD) using a D/max-2500/PC diffractometer. The nanoindentation of the white reticular microstructure in the surfacing layer was measured using a Hysitron PI-85 nanoindentation tester. The crystal structure of each phase was examined by a JEOL ARM-200F transmission electron microscope (TEM). The phase transformation temperature of the surfacing layer during tempering process was obtained by STA 449C differential scanning calorimeter (DSC). All of the experiments were carried out in State Key Laboratory of China Metastable Materials.

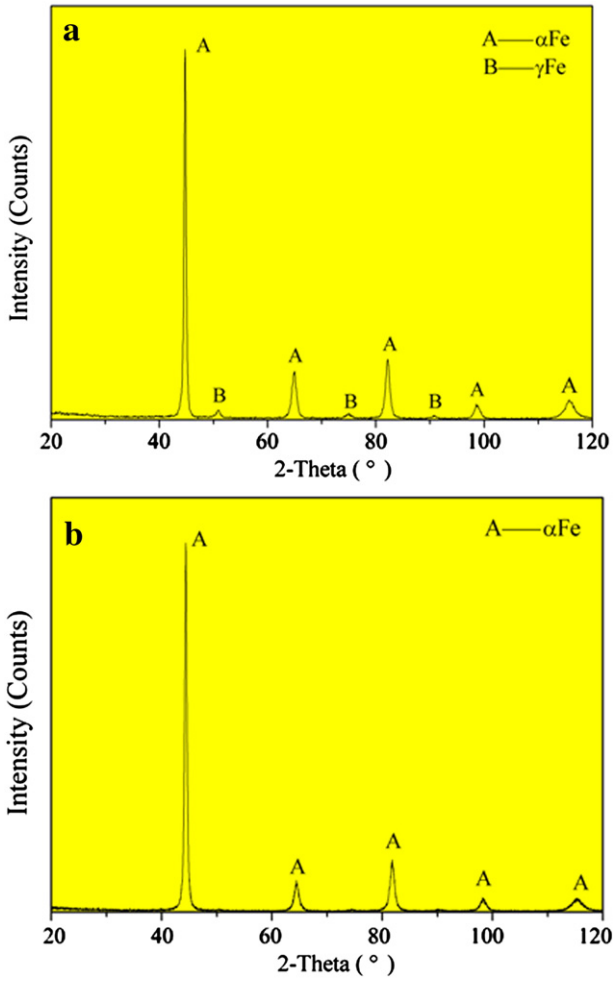

Fig. 3. X-ray diffraction patterns for hardfacing metals tempered at a) 350 °C and b) 650 °C.

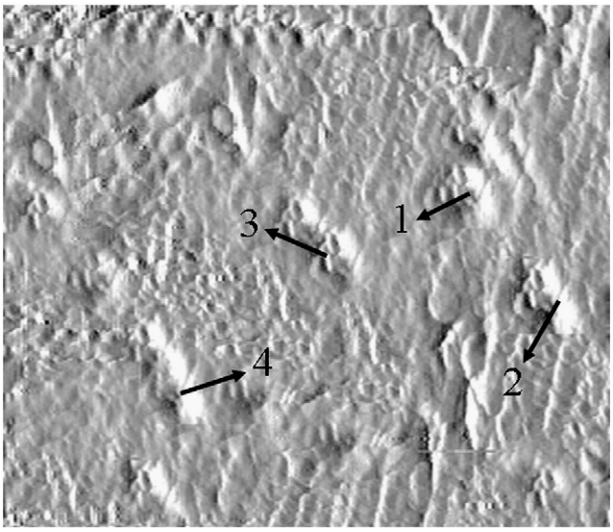

Fig. 4. Nanoindenting hardness graph of the hardfacing metal tempered at 350 °C.

3. Results and discussions

3.1. Identification of the white reticular microstructure in the surfacing layer

3.1.1. Microstructure and phase structure of the as-welded surfacing layer

The microstructure of the as-welded surfacing layer is shown in Fig. 1(a). From Fig. 1(a), it consists of black needle martensite (the normal martensite), retained austenite and some white reticular microstructures distributed uniformly on the crystal boundary in the surfacing layer.

Fig. 1(b) illustrates the XRD pattern of the as-welded surfacing layer, revealing α-Fe and γ-Fe. Combined with Fig. 1(a), it shows that the microstructure of the as-welded surfacing layer consists of martensite and retained austenite.

3.1.2. Microstructures and phase structures of the surfacing layers at different tempering temperatures

The microstructures of the surfacing layers tempered at different temperatures, 350 °C, 450 °C, 550 °C, and 650 °C, respectively, are shown in Fig. 2. When the tempering temperature is 350 °C, tempered

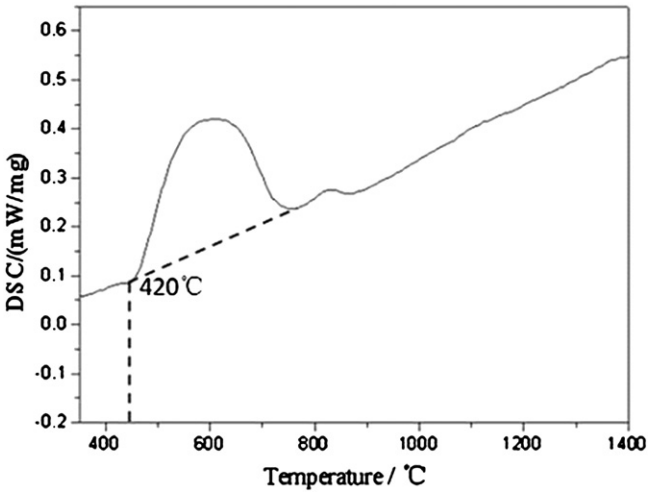

Fig. 5. DSC curve of the hardfacing metal on the heating process after quenched.

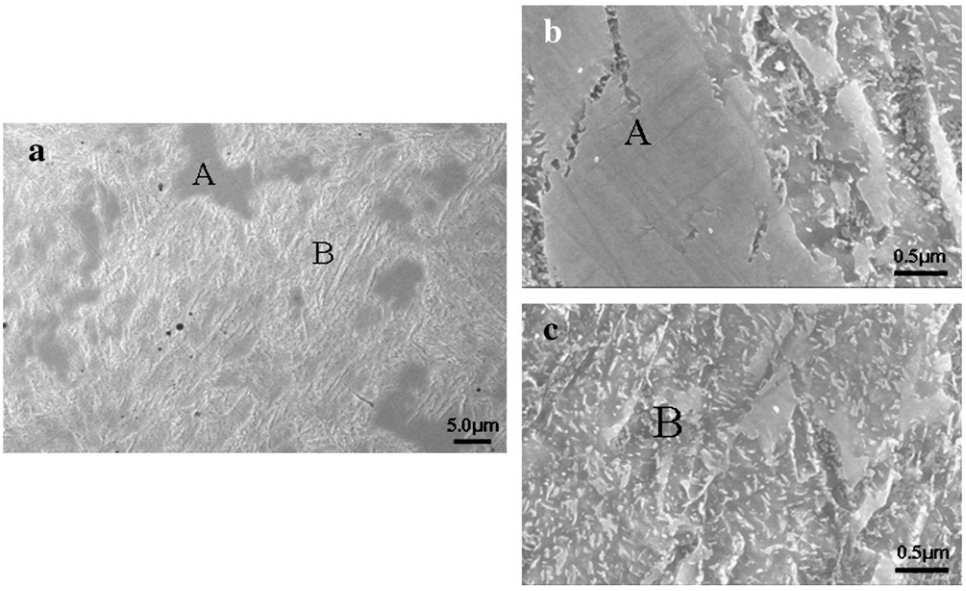

Fig. 6. FESEM of a) hardfacing metal, b) white reticular martensite and c) normal martensite.

needle-shaped martensite and a little retained austenite can be found in the grains, while the white reticular microstructure is distributed on the crystal boundary obviously. With increase of the tempering temperature, as shown in Fig. 2(b), (c) and (d), the white reticular microstructure decreases gradually. When the tempering temperature is 650 °C, the white reticular microstructure dissolves completely and is replaced by the black one.

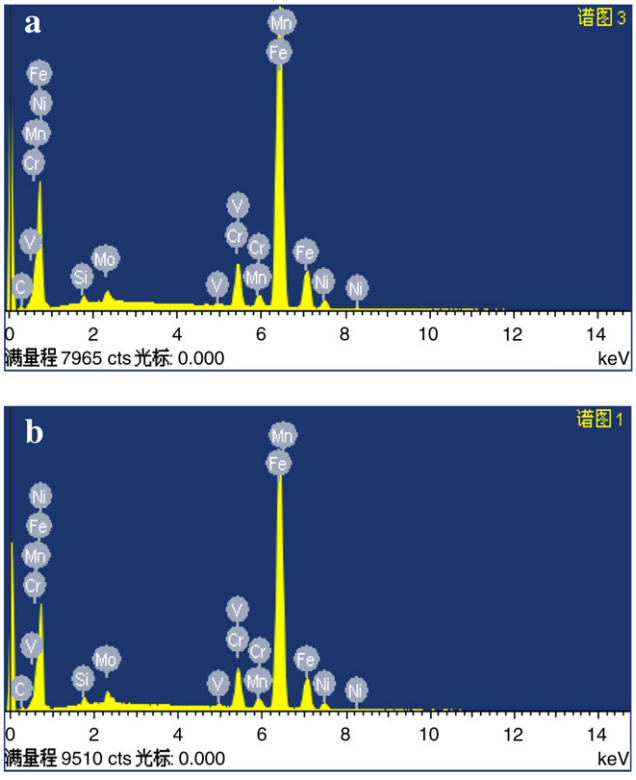

Fig. 7. EDS of a) white reticular martensite and b) normal martensite in hardfacing metal.

Fig. 3 illustrates the X-ray diffraction patterns for the surfacing metals tempered at 350 °C and 650 °C. As shown, when the tempered temperature is 350 °C, α-Fe and γ-Fe exist in the surfacing layer, in which the γ-Fe is retained austenite and the α-Fe may be either the martensite without transformation or the tempered martensite after transformation. When the tempered temperature reaches 650 °C, γ-Fe disappears completely, only α-Fe exists in the surfacing layer.

From Fig. 2, it can be seen that a large amount of white reticular microstructure exists in the surfacing layer tempered at 350 °C, whose amount decreases gradually with increase of the tempering temperature. When the tempering temperature is 650 °C, it disappears completely. As well known, the temperatures, at which carbides start to dissolve is above 1000 °C [15,16], which means that it is impossible for the white reticular microstructure to dissolve in matrix when the temperature increases from 350 °C to 650 °C, so the white reticular microstructure could be retained austenite or martensite, instead carbides.

3.1.3. Nanoindentation of the surfacing layer

Fig. 4 illustrates the nanoindentation graph of the white reticular microstructure existing in the surfacing layer after tempered at 350 °C. Four points were tested and the average nanoindentation of the white reticular microstructure is 14.33 GPa.

J.M. Jungk [17] indicated that the nanoindentation range of martensite was from 13.45 GPa to 15.47 GPa and that of retained austenite was from 2.78 GPa to 4.89 GPa. It is obvious that the nanoindentation of the white reticular microstructure is among the range of martensite, rather than retained austenite, so it can indentify that the white reticular microstructure is martensite instead of retained austenite.

Table 4
Chemical compositions of white reticular martensite and normal one in hardfacing metal as-welded (wt.%).

Elements	C	Si	S	P	Cr	Mn	Ni	Mo	V	Fe
White reticular martensite	2.14	1.88	0.31	0.27	7.34	3.66	3.56	2.44	0.89	Balance
Normal martensite	1.28	2.01	0.42	0.58	6.14	2.85	2.92	1.84	0.68	Balance

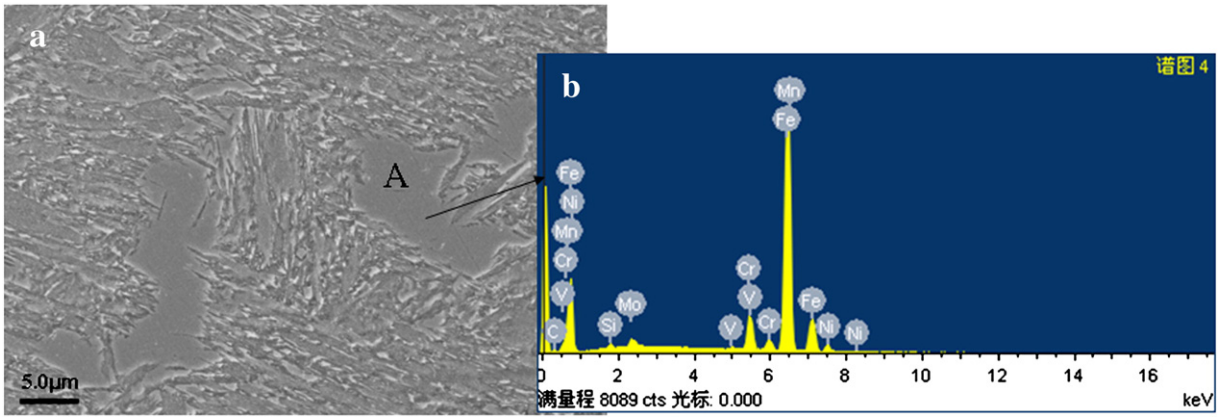

Fig. 8. a) FESEM and b) EDS of high-alloy martensite in hardfacing metal tempered at 650 °C.

3.2. Characterization of the high-alloy martensite in the surfacing layer

3.2.1. DSC curve of the surfacing layer

Fig. 5 illustrates the DSC curve determined during the tempering process after quenching. As shown in Fig. 5, a clear exothermic peak appears on the DSC curve when the tempering temperature is 420 °C. Combined with Fig. 2, it can be concluded that the temperature at which the martensite starts to dissolve is 420 °C.

Table 5
Chemical compositions of high-alloy martensite and normal one tempered at 650 °C (wt.%).

Elements	Si	S	P	Cr	Mn	Ni	Mo	V	Fe
White reticular martensite	2.21	0.33	0.42	5.78	2.42	2.87	1.86	0.57	Balance
Normal martensite	1.94	0.28	0.52	6.21	3.04	3.13	2.05	0.72	Balance

3.2.2. FESEM of the surfacing layer

Fig. 6 shows the FESEM of the as-welded surfacing layer. From Fig. 6, white reticular martensite is lamellar, while the normal one is irregular needle. In order to analyze the difference in composition of the two kinds of martensites, EDS analysis was used. Fig. 7 illustrates the EDS of the above mentioned martensite, and Table 4 presents the corresponding data. As shown in Fig. 7 and Table 4, besides the content of C, the contents of alloy elements such as Cr, Mn, Ni, Mo, and V in white reticular martensite are clearly higher than those in normal martensite, so the white reticular martensite is taken as high-alloy martensite.

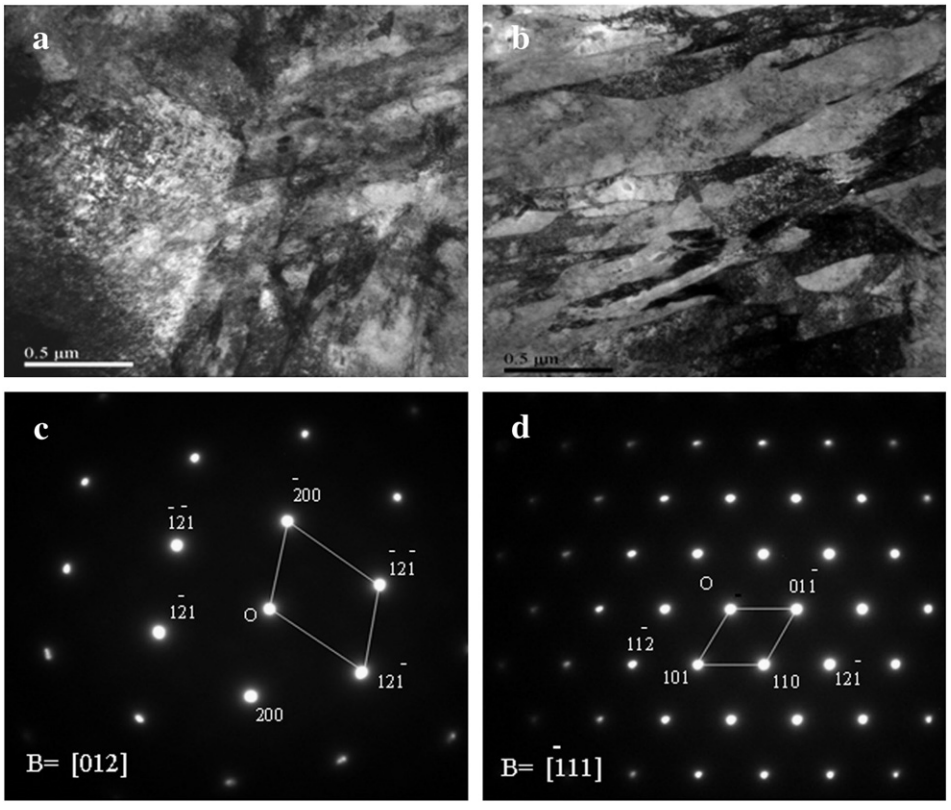

Fig. 9. High resolution transmission electron micrographs and Diffraction patterns of a), c) high-alloy martensite and b), d) normal martensite.

Table 6
Distances of $\left(12\bar{1}\right)$ lattice plane and lattice constants of the high-alloy martensite and the normal one.

	Distance of $\left(12\bar{1}\right)$ lattice plane/Å	Lattice constant a/Å	Lattice constant c/Å
High alloy martensite	1.1748	2.846	3.053
Normal martensite	1.1734	2.854	2.983

Fig. 8 demonstrates the FESEM and EDS of the high-alloy martensite in the surfacing layer after tempered at 650 °C. In Fig. 2(d), which was observed by OM, the white reticular high-alloy martensite is replaced by the black one. However, compared with Figs. 6(a) and 8(a), the morphology does not change obviously of the high-alloy martensite when the tempering temperature is 650 °C.

The compositions of the high-alloy martensite and normal one tempered at 650 °C are listed in Table 5. Compared Table 4 with Table 5, the high-alloy martensite tempered at 650 °C contains the lower alloy content than that tempered at 350 °C. The total content of all alloy elements decreases from 17.89% to 13.5%, among which the Cr content decreases the most significantly. In contrast, the content of alloy elements in the normal one increases slightly.

The higher Cr content of high-alloy martensite leads to its excellent corrosion resistance, so the high-alloy martensite is bright in as-welded surfacing layer. With increase of the tempering temperature, the high-alloy martensite dissolves gradually, accompanied by deteriorating corrosion resistance due to the decreases in Cr content. Therefore, the high-alloy martensite distributed on the crystal boundary exists as black reticular morphology with lower corrosion resistance after tempering.

3.2.3. TEM images of the surfacing layer

In order to analyze the difference in lattice types between the high-alloy martensite and the normal martensite, their high resolution transmission electron micrographs in the surfacing layer were observed, which are shown in Fig. 9(a) and (b). Compared with Fig. 2, the high-alloy martensite is reticular when it is observed by lower resolution OM and lumpy by higher resolution TEM. While the normal martensite is needle-like and board-like when they were observed by OM and TEM, respectively.

Fig. 9(c) and (d) illustrates the diffraction patterns of the high-alloy martensite and the normal martensite. After calibrating the diffraction patterns, the structures of the high-alloy martensite and the normal one are both body-centered tetragonal. The distances of $\left(12\bar{1}\right)$ lattice plane and the lattice constants of the two kinds of martensites are calculated, as listed in Table 6, which indicates that the c-axis of the high-alloy martensite is longer than that of the normal one.

4. Conclusion

1. The as-welded surfacing layer consists of martensite and retained austenite. Meanwhile, the high-alloy martensite with white reticular morphology is distributed on the crystal boundary. When the tempering temperature is 350 °C, no phase transformation occurs in the surfacing layer. However, the high-alloy martensite disappears gradually with the increase of the tempering temperature, and finally appears as a black network when the tempering temperature is 650 °C.
2. The nanoindentation hardness of the high-alloy martensite is 14.33 GPa and the high-alloy martensite starts to dissolve in the matrix at 420 °C.
3. The high-alloy martensite is lumpy while the normal one is board-like when they are observed by TEM. The alloy element content of the high-alloy martensite is higher than that of the normal martensite. After tempering at 650 °C, the morphology of the high-alloy martensite does not change obviously, while the total content of alloy element decreases rapidly.
4. Both the high-alloy martensite and the normal one are body-centered tetragonal. The lattice constants c of them are 3.053 Å and 2.983 Å, respectively, which shows that the c-axis of the high-alloy martensite is longer than that of the normal one.

References

[1] A. Nassir, B. Ali, J Mater Process Technol 210 (2010) 1364.
[2] M. Pellizzari, A. Molinari, G. Straffelini, Wear 259 (2005) 1281.
[3] C. Fan, M.C. Chen, C.M. Chang, W. Wu, Surf CoatTechnol 201 (2006) 908.
[4] V.E. Buchanan, D.G. McCartney, P.H. Shipway, Wear 264 (2008) 542.
[5] X.W. Qi, Z.N. Jia, Q.X. Yang, Y.L. Yang, Surf CoatTechnol 205 (2011) 5510.
[6] A. Kamp, S. Celotto, D.N. Hanlon, Mater Sci Eng A 538 (2012) 35.
[7] J.M. Brossard, M.P. Hierro, J.A. Trilleros, M.C. Carpintero, L. Sánchez, F.J. Bolívar, F.J. Pérez, Surf CoatTechnol 201 (2007) 5743.
[8] R.R. DeAvillez, Mater Sci Eng A 63 (1984) L9.
[9] S. Saduman, Surf CoatTechnol 190 (2005) 1.
[10] E. Yasar, E. Güler, H. Güngünes, T.N. Durlu, Mater Charact 59 (2008) 769.
[11] K. George, Mater Sci Eng A 273-275 (1999) 40.
[12] H. Matsumoto, H. Yoneda, D. Fabregue, E. Maire, A. Chiba, F. Gejima, J Alloys Compd 2 (2011) 2684.
[13] E.J. Petit, Y. Grosbety, S. Aden-Ali, J. Gilgert, Z. Azari, Surf CoatTechnol 205 (2010) 2404.
[14] H.B. Zheng, X.N. Ye, L.Z. Jiang, B.S. Wang, Z.Y. Liu, G.D. Wang, Mater. Des. 31 (2010) 4836.
[15] S.S. Shcheka, M. Wiedenbeck, J. Daniel, Earth Planet. Sci. Lett. 245 (2006) 730.
[16] C. Katsich, E. Badisch, Surf CoatTechnol 206 (2011) 1062.
[17] J.M. Jungk, B.L. Boyce, T.E. Buchheit, T.A. Friedmann, D. Yang, W.W. Gerberich, Acta Mater 54 (2006) 4043.